journals.uoz.edu.krd

MAPPING FLOOD VULNERABILITY BY APPLYING EBF AND AHP METHODS, IN THE IRAQI MOUNTAIN REGION

Abdulrazzaq Q. Mikail [a, b*], Rahel Hamad [a,c]

[a] Scientific Research Center, GIS & Remote Sensing Department, Delzyan Campus, Soran University, Soran 44008, Iraq.
[b] Faculty of Science, Delzyan Campus, Soran University, Soran 44008, Iraq (abdulrazaq.mikail@soran.edu.iq)
[c] Faculty of Science, Petroleum Geosciences Department, Delzyan Campus, Soran University, Soran 44008, Iraq.

ABSTRACT

Flood hazards are a member of the world's catastrophic events with a hydrological climate origin. They are referred to as a situation in which the river flows and water level increases suddenly and causes human and financial losses. This research aims to determine flood-prone zones and evaluate the efficacy of RS and GIS-based evidence-based belief function (EBF) and hierarchical analysis (AHP) models in flood-prone area mapping. Using the Rezan River basin in the Mergasor area of Erbil governorate, Iraq, as an example, 11 factors such as slope, slope direction, land use, distance to the stream, distance to the road, elevation, soil, rainfall, geology, NDVI, and drainage density were utilized for flood moderation. The prediction rates of the EBF and AHP models were also analyzed to be 0.869% and 0.836%, respectively, indicating that these two models are better predictors. The findings of the study area revealed that 32% of the study area is under very high to high flooding hazard zones for the EBF method and 22% for the AHP method. This research's conclusions are crucial for flood-prone region management, decision-making, and local administrative planning.

KEYWORDS: Flood Vulnerability, Susceptibility, Hazard, Rezan River, Mergasor.

1. INTRODUCTION

Floods are one of nature's damaging natural catastrophes (Tehrany & Kumar, 2018). Accurately analyzing their hazards is challenging owing to a lack of data and knowledge of flood damage of various magnitudes (Grahn & Nyberg, 2017). Natural catastrophes inflict substantial economic and human losses in human communities. They are caused by natural disasters that provide a severe risk including flooding, drought, earthquake, landslide, cyclones, and volcanos. These incidents do not become natural disasters in regions without straight contact with persons or impact mortal welfare (Fernández & Lutz, 2010).

A brief description of flood events is that it is the rise of the level of water than the necessary level generated by increased surface water in a stream succeeding severe rains, covering the floodplain and surrounding grounds, damaging agricultural and metropolitan areas, and resulting in fatalities (Chapi et al., 2017; Huang et al., 2008). Maps indicating the potential for floods are a valuable tool for determining the future course of urban expansion and are often used to pinpoint these locations (Büchele et al., 2006). Maps of the flood zone and the hazard evaluations for diverse regions comprise numerous criteria items that must be spatially related (Booij, 2005). Floods are frequently caused by a combination of severe meteorological, hydrological, and physical conditions (Chowdhuri et al., 2020). One current and specific case of a flash flood tragedy happened in Erbil, Iraq's Kurdistan region, destroying the city financially and causing human casualties. Erbil city had a massive floods in November and December 2021 as a consequence of severe monsoons in a short time, unmethodical sewerage, and deluge rains, killing 12 people, destroying over 1200 automobiles, and sinking more than 200 dwellings. Thus, flood vulnerability mapping is a critical step in flood relief because it recognizes areas numerously vulnerable to floods and provides enough time to prepare so that people can adapt to flooding predictably rather than retroactively (Zhao et al., 2018) . Several authors investigated some approaches to appreciate the possibilities of these solutions in light of the necessity for an accurate and trustworthy technique to determine floodable places (Rahmati et al., 2016).

Due to its ability to handle enormous amounts of geographical data, the GIS has been proved as an effective instrument for spatial analysis and information handling (Oh & Pradhan, 2011). Many investigators have extensively used a mix of based on analytical models in conjunction with Geographic Information systems and remote sensing (Tehrany & Kumar, 2018). A range of arithmetical and probabilistic methods have been experienced recently for creating flood vulnerability maps (Lee et al., 2012; Levy et al., 2007). The evidential belief function (EBF) technique, for instance, has been used to estimate potential groundwater zones (Althuwaynee et al., 2014) and analyze the vulnerability of landslides (Tien Bui et al., 2018), among other natural catastrophes. It is now infrequently utilized for flood studies (Nampak et al., 2014). In order to estimate flood risk, Chen and Yeh (Chen et al., 2011) employed the AHP and GIS, producing valuable, all-inclusive data for flood risk management in Taiwan. Additionally, other researchers have studied and put into practice a variety of maps of flood susceptibility strategies over the years. Tehrany and Kumar (2018) examined the potent EBF approach in the background map of flood susceptibility. Additionally, when used with logistic regression techniques, Tien Bui and Khosravi showed that the EBF model had the most fantastic accuracy in forecasting flood vulnerability. On the other hand, (Das, 2020) used the AHP approach to create maps of flood susceptibility, sensitivity, and risk for the whole Western Ghat coastline area in India by combining a sizable number of environmental flood conditioning components from various sources.

As a result, different locations need different aspects for flood mapping and risk assessments (Poussin et al., 2014). As a result, multi-criteria decision analysis (MCDA) methods have been successfully used in several research and are now commonly regarded as a helpful tool for evaluating complex choice situations (Cinelli et al., 2014; Hongoh et al., 2011). Additionally, MCDA considers various factors, such as technical, environmental, and socioeconomic factors, to reach a flawless conclusion (Mühlbacher & Kaczynski, 2016). Furthermore, a GIS-based MCDA was utilized to map flood regions (Dash & Sar, 2020), owing to the simplicity with which GIS methods facilitate spatial data handling and analysis and the convenience with which the MCDA result may be seen, interpreted, and evaluated (Hammami et al., 2019).

Validation is crucial when making maps of vulnerability to natural disasters for use in planning (Khosravi et al., 2016). In reality, a study of flood vulnerability and verification of the resulting map for accessibility and implementation mistakes has to be conducted. Furthermore, confirming the prediction outcome is essential due to the significant interpretation that researchers obtain from the prediction outcome (Shariat et al., 2010).

The primary goals of the study were to (1) assess the efficacy of EBF, and AHP approaches to generate a map of flood susceptibility and (2) pinpoint the region's most vulnerable to river flooding, a phenomenon that frequently causes significant property and infrastructure damage, injuries, and fatalities in mountainous regions. In order to do this, a number of GIS-based patterns are used and assessed in the Mergasor district's Rezan river drainage area.

2. STUDY AREA

The research region is about 175 kilometres northeast of Erbil, Iraq, between 36°41'6.53 and 37° 2'7.13 N latitudes, 44°18'53.20 and 43°38'36.59 E longitudes. The drainage region covers the Baze, Barzan, Rezan, Bele, and Mergasor districts bordered by Turkey. The elevation spans from 402 to 2292 meters higher than the *Sea-level*, and the climate is described as having the Mediterranean climate with an average annual precipitation of 1042 mm. The wettest months are November through April, extending approximately from 250 to 400 mm. The rainy season, with its heavy rainfall combined with topographical conditions, can cause flooding. The moderate annual temperature in the basin varies from 22° to 26°, with the lowest and highest temperatures meandering from 5° to 12° and 35° to 40°, separately. The research area is 55 kilometres lengthy and 25 kilometres vast, with a whole area of 1173 km2, and it has both flat and hilly topography (Figure 1).
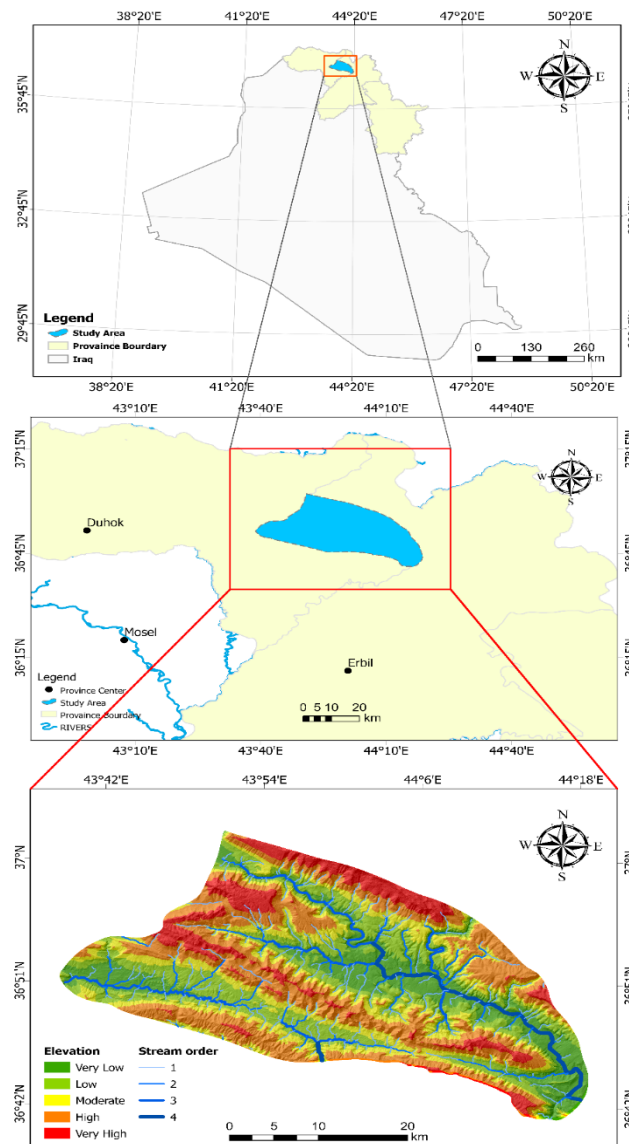

Figure 1. The investigation region location map.

3. MATERIALS AND METHODS

3.1 Data Set

Many distinct flood variables have been noticed and employed by researchers. For this research, numerous geographical characteristics that impact floods were evaluated, like the elevation, geology, soil type, land use, aspect, distance to the road, distance to the river, NDVI, slope, precipitation, and drainage density. Using data from the Advanced Land Observing Satellite-PALSAR, a DEM kindled with the 12.5m resolution was employed to obtain relevant parameters like slope, streams, aspect, and hillside objects. The geological map of the investigation region was obtained from the Iraqi Geological Survey. Furthermore, we identified the best geochronological after applying geological and climatic data in combination with modeling approaches and expert opinion. Finally, the SWAT tool lets users prepare canals and basins within a watershed to prioritize protecting multiple water quality objectives. This GIS tool helps researchers see what is causing local water quality problems. The data utilized in the study are all shown in Table 1.

vulnerability map that can be used to predict flooding (Park, 2011). The EBF method contains four fundamental purposes with values ranging from 0 to 1: Bel (belief function) , Dis (disbelief function) , Unc (uncertainty function) , and Pls (possibility function) (Chowdhuri et al., 2020) . The pictorial representation of these combinations is depicted in Figure 2.
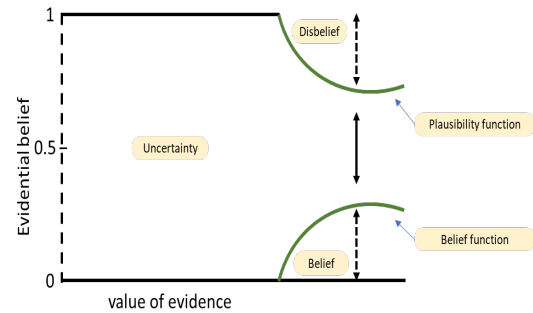

Figure 2: Illustrates the links between the evidential belief functions.

The value of the Bel method represents a "pessimistic" estimate, while the value of the Pls method is represented an "optimistic"

Table 1. Displays the multiple data sets that were applied to produce flood vulnerability mapping

Data Description	Data used	Data Source	Resolution	Data Types
LULC and NDVI	Sentinel 2A Multispectral Instrument (MSI) images (Accusation date: 16 July 2021	European Space Agency (ESA) earth online	10 m	Grid / Polygon
NDVI= $\frac{NIR-RED}{NIR+RED}$	Sentinel 2A Multispectral Instrument (MSI) images (Accusation date: 16 July 2021	European Space Agency (ESA) earth online	10 m	Grid / Polygon
Basin boundary, DEM, Hill-shade, Drainage Density, Slope, Lineament Density distance to river and road	Advanced Land Observing Satellite (ALOS) - Phased Array type L-band Synthetic Aperture Radar (PALSAR)	ALOS ｜ ALOS@EORC (jaxa.jp)	12.5 m	Grid / Polygon /point
Geological map	26 geological units	Geological survey (Baghdad)	1:1000000	Grid / Polygon
Soil types	Soil map	Exploratory Soil Map of Iraq, Scale 1:1,000,00	1:1000000	Grid / Polygon
Rainfall	Annual rainfall data from 2000 to 2020	Erbil and Duhok Meteorological Office	12.5 m	Grid / Polygon /point

3.2 Evidential Belief Function (EBF)

Shafer first presented the Dempster–Shafer evidence theory, which represents a mathematical model consisting of logical and belief-relevance heuristics, which is perceived as spatial integration (Shafer, 1976). It is a reasonable or helpful concept or method used to extract knowledge from data. The Dempster-Schafer method's stability is handling data that aren't complete. There have shown that the conclusion of belief, disbelief, uncertainty, and plausibility should be as precisely specified as possible; in this way, a favourable outcome may be achieved (Carranza, 2009). The EBF approach is the best modern flood vulnerability assessment and mapping method (Tehrany & Kumar, 2018). Depending on the data source, an EBF approach can be computed using the data-based or knowledge-based approach (Mondal & Mandal, 2020).

The data-driven EBF model will be used in the flood vulnerability study and will be viewed as a multivariate statistical investigation since it considers the geographical relationship between each causative element and flood classes (Carranza et al., 2005). Because of its great accuracy and flexibility, researchers are increasingly turning to the data-driven Dempster-Shafer EBF method to generate a flood vulnerability map. The first step to using this method is to convert it to data layers and then combine those layers, which, after this method is completed, create a flood

assessment of the spatial association during the flood. However, it also discusses the factors that affect these results to illustrate a complete understanding of this analysis (Awasthi & Chauhan, 2011; Pradhan & Althuwaynee). Consequently, the Bel value is either a lower or the same amount compared to Pls. The distinction between the value of Pls and Bel methods is the Unc value, which shows that the theory is founded on ignorance or unawareness of evidence. In contrast, the Dis value refers to the idea that a theory is incorrect as a consequence of evidence (Awasthi & Chauhan, 2011; Azadi et al., 2020; Tien Bui et al., 2019). Before employing the model, collect flood conditioning variables and flood inventory data (training dataset) to get the essential quantitative information. This investigation used 33 validation data points, 77 training data points, and eleven influencing factors. The following instructions provide a data-driven estimate of Bel, Dis, Unc, and Pls : (Althuwaynee et al., 2012; Carranza & Hale, 2003).

$$\beta = 1 - \sum_{i-2}^{n} (\text{Bel}_{i-1} \, \text{Dis}_i - \text{Dis}_{i-1} \, Bel_i) \qquad (1)$$

$$\text{Belief} \,(Bel) = \frac{Bel_1 + Bel_2 + \cdots \ldots + Bel_n}{\beta} \qquad (2)$$

$$\text{Disbelief} \,(\,\text{Dis}\,) = \frac{\text{Dis}_2 + \text{Dis}_2 + \cdots, + \text{Dis}_n}{\beta} \qquad (3)$$

Uncertainty(Unc)

$$= \frac{\sum_{i=2}^{n}(Unc_{i-1}Unc_i + Bel_{i-1}Unc_i + Bel_iUnc_{i-1} + Dis_{i-1}Unc_i + Dis_iUnc_{i-1})}{\beta}$$

$$(4)$$

Plausibility (Pls) = Bel + Unc $\qquad\qquad$ (5)

where β, which ensures that Bel + Dis + Unc = 1, because this value must always be equal to 1.

3.3 Analytic Hierarchy Process (AHP)

The Analysis Hierarchy Method (AHP) technique is a powerful and flexible multi-criteria decision-making method that can solve complex problems at different levels. For this reason, it is called a hierarchy model because it is entered in the form of a tree model and levels (Saaty, 1977). The AHP method combines both objective and subjective evaluations in an integrated structure based on scales with paired comparisons. It helps analysts to organize the essential aspects of a problem in a hierarchical format (Thomas & Doherty, 1980). Using the AHP approach, users and planners may quantify their preferred scale generated from various possibilities (Ayalew & Yamagishi, 2005). In this work, the weights of all input items for flood risk mapping were determined using AHP. In terms of weight importance, the pairwise comparison matrix was created initially with the help of local experts. In order to create the normalized matrix , each pairwise comparison matrix element was divided by the total of each column. The moderate weight of each row was used to generate the absolute weight value of the corresponding parameter. The consistency ratio (CR) was determined to gauge the level of consistency between the weight values of different factors in order to evaluate the validity and applicability of the importance value calculation procedure, Equation (6). The pairwise comparison matrix is appropriate if Consistency Index (CI) values are comparable to (equal or smaller than) (0.1). However, the matrix should be re-evaluated when the Consistency Index (CI) is greater than (0.1). Equation 7 is employed to obtain the Consistency Index (CI).

$$CR = \frac{CI}{RI} \qquad\qquad (6)$$

$$CI = \frac{\lambda_{max} - n}{n - 1} \qquad\qquad (7)$$

Where $\qquad$ CR: Consistency ratio
$\qquad\qquad$ CI: Consistency Index
$\qquad\qquad$ λ: Eigenvalue
$\qquad\qquad$ n: the order of the matrix
$\qquad\qquad$ RI: Random Consistency Index.

The final CR value must be less than (0.10) for the criterion weights to be valid. Conversely, a high (>0.10) value indicates contradictory judgments that require re-estimating the consequences.

3.4 Validation

Since the ROC curve is a thorough, acceptable, and graphically displayed validation approach, it will be employed to accurately evaluate the flood vulnerability map in this research. Many authors have employed the ROC curve for precision inspection and validation. The area beneath the curve is excellent when the AUC value ranges between 0.9 and 1.0. Also, perfect when the value is between 0.8 and 0.9. The AUC value will be good when it is between 0.7 and 0.8 (Chowdhuri et al., 2020). Moreover, no globally acknowledged approach exists for separating inventory data into training and validation data (Yariyan et al., 2020). As

the methods for organizing inventory data are inconsistent, there is no universally accepted approach in natural hazard evaluations for describing the ratio of inventory data used for training and validation. However, the general split ratio for classifying inventory data in the literature concerning natural hazard assessments is 70/30 (Li & Chen, 2019). The 70/30 ratio will be implemented for splitting datasets in this investigation.

4. RESULTS AND DISCUSSION

4.1 Evidential Belief Function (EBF)

Since most floods are brought on by flooding the primary river trough, distance from the river is one of the essential elements in the flood sensitivity analysis. According to (Appendix, Table A1), the 0-50 m class in the present investigation had the greatest Bel of 0.495 and the lowest Dis of 0.099. Nevertheless, the flood danger Bel values were 0.184, 0.196, 0.126, and 0.000 for the other four classes. Additionally, it shows that lower elevations, with a range of 402 to 800 meters, had bigger Bel values, with the greatest Bel of 0.402 and the lowest Dis of 0.129, showing the highest flooding vulnerability when water flows into and meets lower locations. The EBF data has verified that most floods happen at lower elevations, which makes flooding at higher altitudes very unlikely. Bel is highest, and dis is lowest, 0.343 and 0.150, indicating that the risk of flooding is greatest for slopes from 0° to 15°, followed by the range from 45° to 60°, and then the content from 30° to 45°. Nevertheless, the southwest in the aspect situation has the highest Bel value of 0.244 and the smallest Dis value of 0.107, implying that this category has positive spatial associations with floods. In contrast, the other Bel values are significantly small, indicating a low likelihood of floods. This indicates that floods are likely to occur since the earth rapidly gets saturated due to heavy rain. Likewise, water and barren terrain are represented by negative values and 0, grassland by 0.2-0.4 NDVI values, and forest by values greater than 0.5 (Chowdhuri et al., 2020). The first rainfall class with 900–1000 mm had the highest Bel and the lowest Dis values. As a result, vegetation catches more precipitation. Less water is available to flow over the surface of the ground.

Regarding geological factors, the river terraces had the greatest Bel and Dis values of 0.219 and 0.052, correspondingly. As for soil factors, the chestnut type includes the highest Bel value of 0.448 and Dis value of 0.192, observed by the Lithosols-Chromic cambisols and Calcaric Regosols . At the same time, the Bel amount for the Rough class was 0. Contrarily, land use is vital in averting flooding that endanger human lives, homes, property, and ways of making a living. So, depending on how land is used, the danger of flooding may go down or up. The consequences of the present analysis showed that accounting for 0.415 of the overall land use, the areas used for water sites in the region had the highest Bel values. Similar to how they harm roadways, floods can worsen dangerous flood situations. The most excellent Bel value 0.333, and the lower Dis value 0.124, were produced by separating the roadways, ranging from 0 to 25 m. The consequence was a greater chance of flooding in the regions nearest to the highways. More extensive basins usually get more precipitation than smaller basins, which causes higher runoff. In areas with a larger drainage density (number of streams), rainfall accumulation occurs more quickly, shortening the lag time. The highest Bel value was 0.323, and the lowest Dis value was 0.1450 for the drainage density category. Figure 3 illustrates flood hazard maps for the research area for the EBF method.
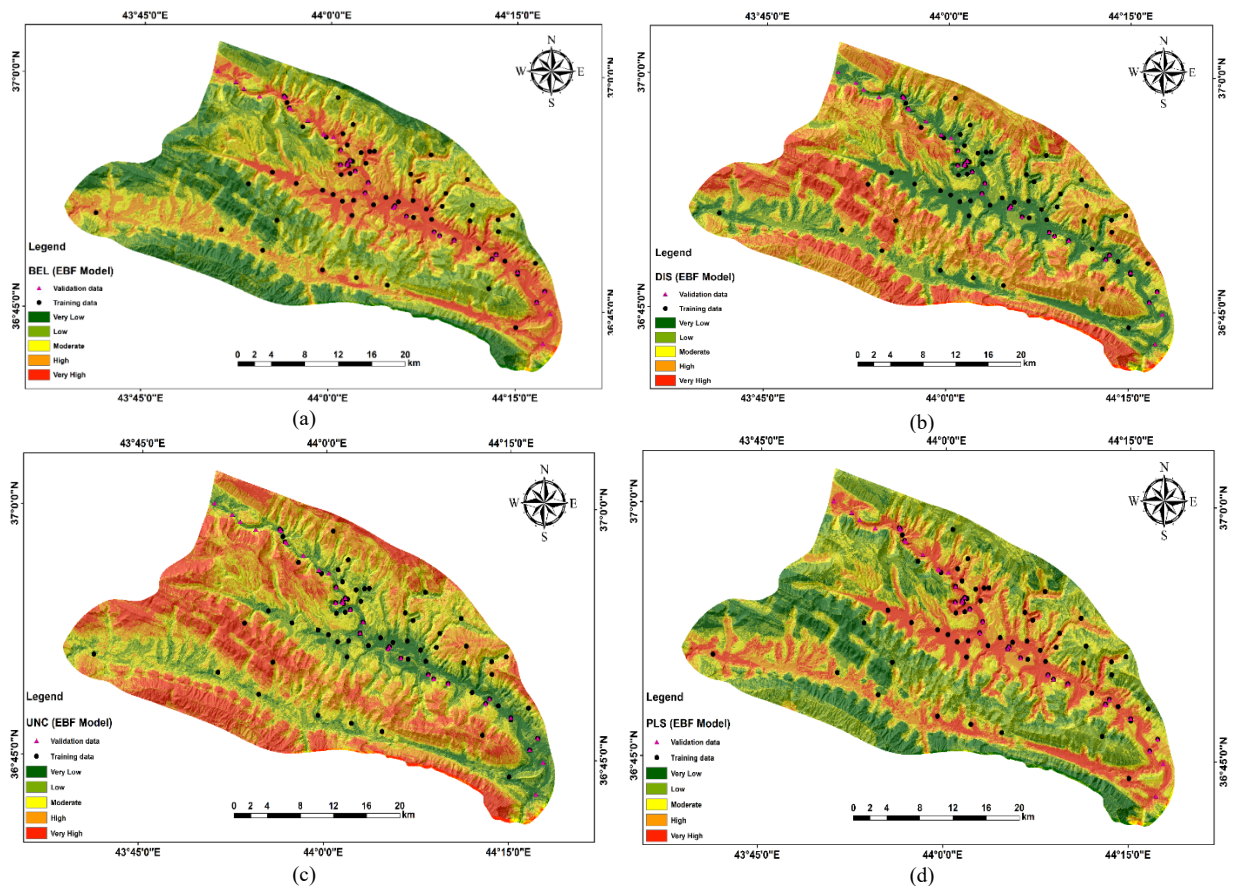
Figure 3. Flood hazard map of the investigation region employing the (a) Bel (degree of belief); (b) Dis (degree of disbelief); (c) Unc (degree of uncertainty); and (d) Pls (degree of plausibility).

4.2 Analytic Hierarchy Process (AHP)

After creating a pairwise comparison matrix, the AHP was utilized to determine the comparative relevance of the relevant components. Weights were assigned to each parameter once rated in order of importance. The comparative importance rating hierarchy varies from 1 to 9, with lower scores meaning lower priority and more elevated scores indicating higher priority. Table 2 displays the pairwise comparison matrix as an 11 x 11 matrix with diagonal components equal to 1. The comparative relevance of each row is calculated by comparing it to each column. For instance, the slope obtains a 3 grade since it is much more critical from the aspect. The row has the reverse value of the pairwise comparison (e.g., 1/3 for aspect) since it represents the importance of each element.

The final column [weight%] of (Appendix, Table A2), shows the percentage contribution of each class to risky regions. The ratio per category was derived by dividing the total weight of the factors by the total weight of the elements. For instance, the first and second rows highlight how significant the slope angle is a comparison to the different classes of slope angle. The flood probability column gives a ratio of 38% to the slope angl class ranges from 0^0 and 15^0, which is significantly additional crucial than the other slope categories. Nevertheless, the different categories of slope angles in the row are fewer significant for the likelihood of flooding. The AHP method's normalized weights are shown in Table 3. The consistency ratio was used to assess the consistency of the element class importance, and the results for all parameter importance ratings are shown in (Appendix, Table A2), The deviations among all factors are approved when the CR value for all element categories is smaller than 0.1. The pairwise comparative trend results show that increases in slope angle, elevation, and NDVI reduce the likelihood of flooding. According to the results concerning different characters, the probability of flooding decreases when the space between the road and the riverbed widens. Other factors, such as drainage density, rainfall, and the various geological formations, increase the probability of flooding.

Table 2. Pairwise comparison matrix by AHP

Factors	Slope	Aspect	Elevation	Rainfall	D.Density	D.River	Land use	NDVI	D.Road	Geology	Soil
Slope	1	3	2	1/2	1/2	1/2	1/3	1/3	3	1/3	1/4
Aspect	1/3	1	1/2	1/3	1/3	1/2	1/3	1/3	1/3	1/5	1/5
Elevation	1/2	2	1	1/3	1/2	1/3	1/2	1/2	2	1/5	1/4
Rainfall	2	3	3	1	3	2	1/2	1/3	3	1/2	1/2
D.Density	2	3	2	1/3	1	1/2	1/2	1/2	2	1/3	1/3
D.River	2	2	3	1/2	2	1	3	2	3	1	1/2
Land use	3	3	2	2	2	1/3	1	1/2	2	1/3	1/4
NDVI	3	3	2	3	2	1/2	2	1	4	2	1/2
D.Road	1/3	3	1/2	1/3	1/2	1/3	1/2	1/4	1	1/4	1/5
Geology	3	5	5	2	3	1	3	1/2	4	1	3
Soil	4	5	4	2	3	2	4	2	5	1/3	1

Table 3. Normalized Pairwise comparison matrix by AHP for eleven factors weight

Factors	Slope	Aspect	Elevations	Rainfalls	D. Density	D. River	Land use	NDVI	D. Road	Geology	Soil
Slope	1.00	3.00	2.00	0.50	0.50	0.50	0.33	0.33	3.00	0.33	0.25
Aspect	0.33	1.00	0.50	0.33	0.33	0.50	0.33	0.33	0.33	0.20	0.20
Elevation	0.50	2.00	1.00	0.33	0.50	0.33	0.50	0.50	2.00	0.20	0.25
Rainfall	2.00	3.00	3.00	1.00	3.00	2.00	0.50	0.33	3.00	0.50	0.50
D. Density	2.00	3.00	2.00	0.33	1.00	0.50	0.50	0.50	2.00	0.33	0.33
D.River	2.00	2.00	3.00	0.50	2.00	1.00	3.00	2.00	3.00	1.00	0.50
Land use	3.00	3.00	2.00	2.00	2.00	0.33	1.00	0.50	2.00	0.33	0.25
NDVI	3.00	3.00	2.00	3.00	2.00	0.50	2.00	1.00	4.00	2.00	0.50
D.Road	0.33	3.00	0.50	0.33	0.50	0.33	0.50	0.25	1.00	0.25	0.20
Geology	3.00	5.00	5.00	2.00	3.00	1.00	3.00	0.50	4.00	1.00	3.00
Soil	4.00	5.00	4.00	2.00	3.00	2.00	4.00	2.00	5.00	0.33	1.00

Flooding likelihood and effect are also affected by the hydrological action of the soil. Flooding is less likely when the soil has a high-water permeability. It is determined by the grain size of the clay and the diameter of the pores in that clay. Thus, clay has poor permeability and a high-water retention capacity.

The AHP flood hazard map indicates that places cover 22.18% of the investigation region with a high or very high risk of flooding. The ArcGIS 10.4 software's reclassification function was used to pre-process all of the requirements as raster datasets while outlining each need in detail. After grade, established the authorities' belief in soil administration, Geological composition, risk administration, and local presidency and experts, their weights were judged utilizing AHP. Through multi-tests reasoning, the weightage undeviating consolidation technique of AHP created a last flood vulnerability map, Figure 4, by calculating all raster's maps cautiously promoting the raster computer in the geographical reasoning. The WGS84/UTM/Zone 38 North coordinate system was employed in the ArcGIS 10.4 software environment to study all the significant sub criteria affecting flooding in the study area. A final flood risk area map was created and classified into five classes of flood risk (very low, low, medium, high, and very high).

4.3 Flood Causative Factors

The study region's location and features were considered while selecting the flood conditioning parameters. Flood vulnerability mapping was created using EBF and AHP methods, which integrated the eleven causative factors: elevation, soils type, drainages density, distanced tor the driver, distanced tor the broad, NDVI, rainfall, aspect, land use, slope, and geology. Weights were determined for each category of flood conditioning factor. It was discovered that areas with highest Bel values and lowest Dis values were the most susceptible to flooding by the EBF approach and, at the same time, generated a map of flood vulnerability map with the AHP approach to determine the high-risk zone of flood in the investigation region.

4.4 Validation

The present work employed 77 flood and non-flood datasets for training and 33 for validation to analyze the model's presentation and validate the flood vulnerability map. The EBF model had the highest sensitivity value of the AUC (0.869) in the training dataset, showing a high degree of classification flood pixel performance, followed by AHP (0.836). As a result, the (AUC) values indicate the accuracy of the two methodologies in flood vulnerability maps, as shown in Figure 5.
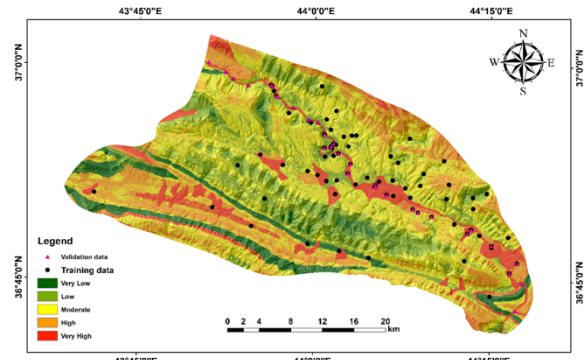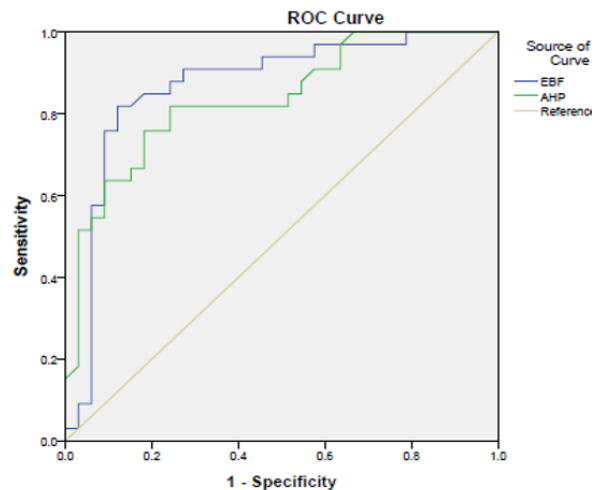

Figure 4. Flood vulnerability map employing AHP.

TEST: EBF: AUC= 0.869   AHP: AUC = 0.836
Figure 5: Receiver operating characteristic (ROC) curve for EBF and AHP methods.

4.5 Further Discussion

4.5.1   Evidential belief function (EBF)

Flood vulnerability mapping was generated using EBF by incorporating elevation, geology, soil type, slope, rainfall, distance to the river, distance to the road, NDVI, land use, drainage density, and aspect. By assigning relative importance to each category of flood conditioning factors, we found that areas with high values for the belief function (Bel) and low values for the disbelief function (Dis) were particularly at risk of flooding. Furthermore, the EBF model's performance was evaluated using the AUC criterion, which indicated that booth training and validating points could map flood vulnerability with an AUC of 0.763 for achievement and 0.869 for forecast rates separately. Our investigation revealed that distanced from the river was a significant factor in determining vulnerability to flooding.

Because of its proximity to the main channel and rapid flood response, the area between 0 and 50 meters in altitude is particularly vulnerable to flooding on the Rezan River. Flooding is more common in riverside communities because of the river's closeness and the fast reaction to flooding, as confirmed by (Chapi et al., 2017; Pham et al., 2020).

Bel values were high (0.448) for both soil type and distance from the river. Several soil properties can affect the volume of runoff in a catchment area (Tehrany et al., 2019). So, the amount of water drains from the ground and causes floods depends on the soil's texture (Fontanine & Costache, 2013). Based on the results of the present investigation, the Chestnut soil class was found (Fontanine & Costache, 2013) to be particularly vulnerable to floods. With a Bel value of 0.297, this soil type suggests it limits precipitation infiltration, leading to more runoff than Lithosols, Rendzinas, and Chromic Cambisols.

For the NDVI, the highest Bel value of 0.426 was found between and (-0.5 to -0.07). According to the results, the likelihood of flooding was the highest in areas with the fewest number of plants. Given their more excellent Bel value and more robust association with floods, these areas were more at risk of flooding than other classes, which is in line with findings from (Chowdhuri et al., 2020).

With a Bel value of 0.415 for the land use component (one of the human disturbance variables), water bodies showed the uppermost chance of flood occurrence. with such an order, Bel values of 0.228, 0.158, 0.143, and 0.057 were recorded for farmland, cities, barren land, and forests. Studies have shown time and time again that changes in land use and land cover have direct or indirect effects on hydrological functions like penetrability (Ossola et al., 2015), evapotranspiration (Wiles & Sharp Jr, 2008), and runoff (Arabameri et al., 2019).

Following the distance of the river, soil type, land use, NDVI, and elevation was the most crucial factor in determining the likelihood of flooding. The category 402 to 800 m elevation range already had the highest value of Bel (0.402) and the smallest value of Dis (0.129) of all the classes, suggesting a greater than average flood risk. In contrast, locations above 2000 m had the smallest Bel value (0.0). These outcomes are in accord with an investigation by (Chowdhuri et al., 2020) in the catchment of eastern India, (Arabameri et al., 2019) they mapped the vulnerability to water risks for northern Iran, and the (Al-Hinai & Abdalla, 2021) investigation in Muscat Governorate , Oman, which determined that only locations at a lower elevation were affected by floods.

Regarding geology, the stream terraces layer had the highest Bel value, 0.219. This was preceded by the Bai Hassan (Upper Bakhtiari) section, which produced 0.171, and the slope sediments formation , which had 0.127. On the other hand, the scores for the different classes show that flooding is not likely to occur because they are lower in Bel and higher in Dis. Slope deposition layers and the river terrace of the Bai Hassan are primarily composed of clastic sedimentary rocks, including conglomerates, sandstone, and claystone, and rock pieces with fine clastic. Generally, the area's geology plays a crucial role in flood inundation mapping due to the involvement of multiple geological formations in hydrological processes. According to (Regmi & Poudel, 2016), they can significantly alter the conductivity and penetrability of water flow.

The soil rapidly gets saturated when rain falls in large amounts, leading to flooding. The rain maps gained weight from EBF verified this. The heaviest rainfall category (900-1000 mm) was assigned: the uppermost Bel value (0.283) and the lowermost Dis value (0.181), indicating that this category experienced the most favourable conditions. So, the more

plants there are, the more rain is collected, while less water is left to run off.

According to EBF's slope-flood study, the slope percentage class 0^0-15^0 produced the uppermost Bel value (0.343) and the lowermost Dis value (0.150). Because of the inverse link between slope and Bel value, the locations with the smallest slope earned the greatest Bel value and the smallest Dis value. Devkota et al., (2013) have drawn connections between land usage, slope, and rainfall depending on their observations in the fields. They explained that land use significantly affected stability of the slope. Forested areas control the flow of water and allow water to seep into the soil at periodic intervals, while agricultural land might compromise stability of the slope owing to much saturated soil.

When considering another human perturbation factor, distance to the road, it is expected that the Bel class has a bigger influence on flooding occurrences the closer the location is near the road. In addition, in regards of the map of distance from the road, the 0-25 m class offered the uppermost Bel value of 0.333 and the lowermost Dis value of 0.124. Furthermore, the impermeable barriers that prevent runoff from percolating into the earth increase the frequency and severity of floods. As a result, roadways in the area under investigation may be harmed, and hazardous flood conditions may arise during a major storm.

The 0.86-1.43 density group was related to the drainage density values, with the greatest Bel value 0.323 and the smallest value of Dis being 0.145. According to the results, this possibility has the best increase in the spring season. (Pourghasemi & Beheshtirad, 2015) confirmed this by noting that the incidence of springs increased with drainage intensity, hence establishing a direct relationship between drainage density and groundwater spring possibility maps. Since rainfall comes sooner in the basin with greater drainage density (number of tributary rivers), leading to a shorter lag time, larger basins receive more rain on the median, resulting in much more discharge.

By contrast, the southeast had the lowest value of 0.107 for the aspect element, and the northwest obtained the greatest value of 0.244. This factor, which also affects the frequency of floods, is vital for wet retention and plant densities. Despite being connected to physiographic elements that, according to (Rahmati et al., 2016), may affect hydrological conditions and soil moisture regimes, the aspect component in the present research had a minor effect on floods. In conclusion, the EBF method found that distance from the river is the essential primary variable contributing equally to flood incidence, then a layer of soil, NDVI, elevation, and land use. But rainfall, aspect, and geology have the most negligible impact on flood danger, followed by slope and distance from the road.

4.5.2   Evidential belief function (EBF)

The hierarchical analysis process (AHP) model has been used in this research to evaluate the determined criteria. By combining GIS facilities and various data, this model is considered a powerful tool in the micro zoning of environmental risks. It weights the criteria based on their importance and impact on creating flood risk by comparing pairs between the requirements. For this purpose, the determining criteria were prepared in pairs and hierarchically in the form of a questionnaire. Finally, after calculating the average of the questionnaires, the data was entered into the special software of the AHP model (Expert choice software), and the relative importance of each criterion was calculated.

According to Tehrany and Kumar (2018), geology has the most weight among the selected layers due to its direct effect on water infiltration and runoff, causing floods. They can substantially impact the conduction and penetration of water flow. Among other factors, the aspect has the least weight due to its immediate impact on flooding compared to other factors. In the next rank are the factors of soil type, NDVI and istance from River, which are assigned more weight due to their influence on the concentration of runoff and its speed. Finally, flood vulnerability mapping was created using the

Table 4. Estimated and actual flooded areas using EBF and AHP approaches.

Vulnerable Zones	EBF method		AHP method	
	Area km^2	Ratio of area (%)	Area km^2	Ratio of area (%)
Very low	211.14	18.00	98.88	8.43
Low	332.89	28.38	335.71	28.62
Moderate	253.48	21.61	478.11	40.76
High	241.98	20.63	196.59	16.76
Very high	133.48	11.38	63.57	5.42

EBF and AHP methods. The risk of flooding has been mapped, and the findings are broken into five categories. The ranges covered here are very low, low, moderate, high, and very high. Table 4 shows that the EBF approach covered a total area of 211.14 (18.00%), 332.89 (28.38%), 253.48 (21.61%), 241.98 (20.63%), and 133.48 (11.38%) square kilometres, respectively, whereas the AHP approach covered a total of 98.88 (8.43%), 335.71 (28.62%), 478.11 (40.76%),196.59 (16.76%), and 63.57 (5.42%) square kilometres, respectively. Accordingly, the research region faces a significant probability of flooding, with over 31% for the EBF model and over 21% for the AHP model. There were high flood susceptibility zones from the junction of the two rivers down to the Rezan River's mouth. The transition between the high and highly high zones constituted the moderate zone. On the other hand, most of the research area is located in areas with a low chance of flooding.

5. CONCLUSIONS

Maps of flood vulnerability might be valuable tools for decision-makers trying to lessen the impact of floods. Here's a rundown of the most important findings:

1. The maps demonstrated that both flood vulnerability models were suitable for making flood hazard classifications. Nevertheless, the EBF model was more effective than the AHP one. Areas with a highest Bel and a lower Dis for flood events are particularly vulnerable, as shown by an examination of flood vulnerability maps.

2. Flood risk may be predicted using slope direction, slope percentage, elevation, soil, proximity to rivers and roads, river density, geology, rainfall, NDVI, and land use. With much of the area under study situated on a mountain plain and steep mountain on all sides, the rapid formation of runoff results in floods in low-slope regions.

This study divided the distance from the river into five categories; the first category (0-25 m) was more vulnerable to flooding, while the chance of flooding decreased with further distance from the river. Also, studies found that the first class, with the lowest elevation, is more likely to experience floods than the other two. Conversely, the first class of NDVI variables includes the increased chance of floods caused by vegetation's absence and vegetation degradation owing to uncontrolled livestock grazing in various portions of the study region.

5.1 Limitation

1. **AHP:** This model uses precise characteristics for judgements. i.e., in practical situations, human emotions are murky, and the leaders may not be able to connect the careful numerical attributes to the examination assessments. AHP is not significant in this case. For creating pairwise correlations, the AHP can only accept free criteria. Because nature is inherently contradictory and decision-making is based only on the situation at hand and the leader's intuition, the AHP cannot take uncertainties and threats into account while a chief is making a decision.

When two criteria or options are examined pairwise, input data are obtained. In any case, the excessive repetition in the correlations is regarded as the reason the pairwise analysis is flawed. Due to the lack of information on the criteria and options and the lack of focus during pairing testing and speaking, AHP allows for irregularity.

2. **EBF:** Lack of required resources specific to the EBF model in flood bora. Most of the studies that have used the model have been conducted on soil erosion.

3. Difficulties in obtaining points in different parts of the study area with GPS due to the high altitudes and difficulties of much of the area to get the necessary data for the study.

REFERENCES

Al-Hinai, H., & Abdalla, R. (2021). Mapping coastal flood susceptible areas using Shannon's entropy model: the case of muscat governorate, Oman. *ISPRS International Journal of Geo-Information*, *10*(4), 252.

Althuwaynee, O. F., Pradhan, B., & Lee, S. (2012). Application of an evidential belief function model in landslide susceptibility mapping. *Computers & Geosciences*, *44*, 120-135.

Althuwaynee, O. F., Pradhan, B., Park, H.-J., & Lee, J. H. (2014). A novel ensemble bivariate statistical evidential belief function with knowledge-based analytical hierarchy process and multivariate statistical logistic regression for landslide susceptibility mapping. *Catena*, *114*, 21-36.

Arabameri, A., Rezaei, K., Cerdà, A., Conoscenti, C., & Kalantari, Z. (2019). A comparison of statistical methods and multi-criteria decision making to map flood hazard susceptibility in Northern Iran. *Science of the Total Environment*, *660*, 443-458.

Awasthi, A., & Chauhan, S. S. (2011). Using AHP and Dempster–Shafer theory for evaluating sustainable transport solutions. *Environmental Modelling & Software*, *26*(6), 787-796.

Ayalew, L., & Yamagishi, H. (2005). The application of GIS-based logistic regression for landslide susceptibility mapping in the Kakuda-Yahiko Mountains, Central Japan. *Geomorphology*, *65*(1-2), 15-31.

Azadi, F., Sadough, S. H., Ghahroudi, M., & Shahabi, H. (2020). Zoning of Flood Risk in Kashkan River basin using Two Models WOE and EBF. *Journal of Geography and Environmental Hazards*, *9*(1), 45-60.

Booij, M. J. (2005). Impact of climate change on river flooding assessed with different spatial model resolutions. *Journal of hydrology*, *303*(1-4), 176-198.

Büchele, B., Kreibich, H., Kron, A., Thieken, A., Ihringer, J., Oberle, P., Merz, B., & Nestmann, F. (2006). Flood-risk mapping: contributions towards an enhanced assessment of extreme events and associated risks. *Natural Hazards and Earth System Sciences*, *6*(4), 485-503.

Carranza, E., Woldai, T., & Chikambwe, E. (2005). Application of data-driven evidential belief functions to prospectivity mapping for aquamarine-bearing pegmatites, Lundazi district, Zambia. *Natural Resources Research*, *14*(1), 47-63.

Carranza, E. J. M. (2009). Controls on mineral deposit occurrence inferred from analysis of their spatial pattern and spatial

association with geological features. *Ore Geology Reviews*, *35*(3-4), 383-400.

Carranza, E. J. M., & Hale, M. (2003). Evidential belief functions for data-driven geologically constrained mapping of gold potential, Baguio district, Philippines. *Ore Geology Reviews*, *22*(1-2), 117-132.

Chapi, K., Singh, V. P., Shirzadi, A., Shahabi, H., Bui, D. T., Pham, B. T., & Khosravi, K. (2017). A novel hybrid artificial intelligence approach for flood susceptibility assessment. *Environmental modelling & software*, *95*, 229-245.

Chen, Y.-R., Yeh, C.-H., & Yu, B. (2011). Integrated application of the analytic hierarchy process and the geographic information system for flood risk assessment and flood plain management in Taiwan. *Natural hazards*, *59*(3), 1261-1276.

Chowdhuri, I., Pal, S. C., & Chakrabortty, R. (2020). Flood susceptibility mapping by ensemble evidential belief function and binomial logistic regression model on river basin of eastern India. *Advances in Space Research*, *65*(5), 1466-1489.

Cinelli, M., Coles, S. R., & Kirwan, K. (2014). Analysis of the potentials of multi criteria decision analysis methods to conduct sustainability assessment. *Ecological indicators*, *46*, 138-148.

Das, S. (2020). Flood susceptibility mapping of the Western Ghat coastal belt using multi-source geospatial data and analytical hierarchy process (AHP). *Remote Sensing Applications: Society and Environment*, *20*, 100379.

Dash, P., & Sar, J. (2020). Identification and validation of potential flood hazard area using GIS-based multi-criteria analysis and satellite data-derived water index. *Journal of Flood Risk Management*, *13*(3), e12620.

Devkota, K. C., Regmi, A. D., Pourghasemi, H. R., Yoshida, K., Pradhan, B., Ryu, I. C., Dhital, M. R., & Althuwaynee, O. F. (2013). Landslide susceptibility mapping using certainty factor, index of entropy and logistic regression models in GIS and their comparison at Mugling–Narayanghat road section in Nepal Himalaya. *Natural hazards*, *65*(1), 135-165.

Fernández, D., & Lutz, M. A. (2010). Urban flood hazard zoning in Tucumán Province, Argentina, using GIS and multicriteria decision analysis. *Engineering Geology*, *111*(1-4), 90-98.

Fontanine, I., & Costache, R. (2013). Using GIS techniques for surface runoff potential analysis in the Subcarpathian area between Buzău and Slănic rivers, in Romania. *Cinq Continents*, *3*(7), 47-57.

Grahn, T., & Nyberg, L. (2017). Assessment of pluvial flood exposure and vulnerability of residential areas. *International Journal of Disaster Risk Reduction*, *21*, 367-375.

Hammami, S., Zouhri, L., Souissi, D., Souei, A., Zghibi, A., Marzougui, A., & Dlala, M. (2019). Application of the GIS based multi-criteria decision analysis and analytical hierarchy process (AHP) in the flood susceptibility mapping (Tunisia). *Arabian Journal of Geosciences*, *12*(21), 1-16.

Hongoh, V., Hoen, A. G., Aenishaenslin, C., Waaub, J.-P., Bélanger, D., & Michel, P. (2011). Spatially explicit multi-criteria decision analysis for managing vector-borne diseases. *International Journal of Health Geographics*, *10*(1), 1-9.

Huang, X., Tan, H., Zhou, J., Yang, T., Benjamin, A., Wen, S. W., Li, S., Liu, A., Li, X., & Fen, S. (2008). Flood hazard in Hunan province of China: an economic loss analysis. *Natural Hazards*, *47*(1), 65-73.

Khosravi, K., Nohani, E., Maroufinia, E., & Pourghasemi, H. R. (2016). A GIS-based flood susceptibility assessment and its mapping in Iran: a comparison between frequency ratio and weights-of-evidence bivariate statistical models with multi-criteria decision-making technique. *Natural Hazards*, *83*(2), 947-987.

Lee, J.-m., Hyun, K.-h., Choi, J.-s., Yoon, Y.-j., & Geronimo, F. K. F. (2012). Flood reduction analysis on watershed of LID design demonstration district using SWMM5. *Desalination and Water Treatment*, *38*(1-3), 255-261.

Levy, J. K., Hartmann, J., Li, K. W., An, Y., & Asgary, A. (2007). Multi-criteria decision support systems for flood hazard mitigation and emergency response in urban watersheds

1. *JAWRA Journal of the American Water Resources Association*, *43*(2), 346-358.

Li, Y., & Chen, W. (2019). Landslide susceptibility evaluation using hybrid integration of evidential belief function and machine learning techniques. *Water*, *12*(1), 113.

Mondal, S., & Mandal, S. (2020). Data-driven evidential belief function (EBF) model in exploring landslide susceptibility zones for the Darjeeling Himalaya, India. *Geocarto International*, *35*(8), 818-856.

Mühlbacher, A. C., & Kaczynski, A. (2016). Making good decisions in healthcare with multi-criteria decision analysis: the use, current research and future development of MCDA. *Applied health economics and health policy*, *14*(1), 29-40.

Nampak, H., Pradhan, B., & Abd Manap, M. (2014). Application of GIS based data driven evidential belief function model to predict groundwater potential zonation. *Journal of Hydrology*, *513*, 283-300.

Oh, H.-J., & Pradhan, B. (2011). Application of a neuro-fuzzy model to landslide-susceptibility mapping for shallow landslides in a tropical hilly area. *Computers & Geosciences*, *37*(9), 1264-1276.

Ossola, A., Hahs, A. K., & Livesley, S. J. (2015). Habitat complexity influences fine scale hydrological processes and the incidence of stormwater runoff in managed urban ecosystems. *Journal of Environmental Management*, *159*, 1-10.

Park, N.-W. (2011). Application of Dempster-Shafer theory of evidence to GIS-based landslide susceptibility analysis. *Environmental earth sciences*, *62*(2), 367-376.

Pham, B. T., Avand, M., Janizadeh, S., Phong, T. V., Al-Ansari, N., Ho, L. S., Das, S., Le, H. V., Amini, A., & Bozchaloei, S. K. (2020). GIS based hybrid computational approaches for flash flood susceptibility assessment. *Water*, *12*(3), 683.

Pourghasemi, H. R., & Beheshtirad, M. (2015). Assessment of a data-driven evidential belief function model and GIS for groundwater potential mapping in the Koohrang Watershed, Iran. *Geocarto International*, *30*(6), 662-685.

Poussin, J. K., Botzen, W. W., & Aerts, J. C. (2014). Factors of influence on flood damage mitigation behaviour by households. *Environmental Science & Policy*, *40*, 69-77.

Pradhan, B., & Althuwaynee, O. Ensemble of data-driven EBF model with knowledge based AHP model for slope failure assessment in GIS using cluster pattern.

Rahmati, O., Pourghasemi, H. R., & Zeinivand, H. (2016). Flood susceptibility mapping using frequency ratio and weights-of-evidence models in the Golastan Province, Iran. *Geocarto International*, *31*(1), 42-70.

Regmi, A. D., & Poudel, K. (2016). Assessment of landslide susceptibility using GIS-based evidential belief function in Patu Khola watershed, Dang, Nepal. *Environmental Earth Sciences*, *75*(9), 1-20.

Saaty, T. L. (1977). A scaling method for priorities in hierarchical structures. *Journal of mathematical psychology*, *15*(3), 234-281.

Shafer, G. (1976). *A mathematical theory of evidence* (Vol. 42). Princeton university press.

Shariat, S. F., Lotan, Y., Vickers, A., Karakiewicz, P. I., Schmitz-Dräger, B. J., Goebell, P. J., & Malats, N. (2010). Statistical consideration for clinical biomarker research in bladder cancer. *Urologic Oncology: Seminars and Original Investigations*,

Tehrany, M. S., & Kumar, L. (2018). The application of a Dempster–Shafer-based evidential belief function in flood susceptibility mapping and comparison with frequency ratio and logistic regression methods. *Environmental Earth Sciences*, *77*(13), 1-24.

Tehrany, M. S., Kumar, L., & Shabani, F. (2019). A novel GIS-based ensemble technique for flood susceptibility mapping using evidential belief function and support vector machine: Brisbane, Australia. *PeerJ*, *7*, e7653.

Thomas, P. G., & Doherty, P. C. (1980). The Analytic Hierarchy. Process: Planning, Priority Setting, Resource Allocation, McGraw-Hill,

Tien Bui, D., Khosravi, K., Shahabi, H., Daggupati, P., Adamowski, J. F., Melesse, A. M., Thai Pham, B., Pourghasemi, H. R., Mahmoudi, M., & Bahrami, S. (2019). Flood spatial modeling in northern Iran using remote sensing and gis: A comparison between evidential belief functions and its ensemble with a multivariate logistic regression model. *Remote Sensing*, *11*(13), 1589.

Tien Bui, D., Shahabi, H., Shirzadi, A., Chapi, K., Alizadeh, M., Chen, W., Mohammadi, A., Ahmad, B. B., Panahi, M., & Hong, H. (2018). Landslide detection and susceptibility mapping by airsar data using support vector machine and index of entropy models in cameron highlands, malaysia. *Remote Sensing*, *10*(10), 1527.

Wiles, T. J., & Sharp Jr, J. M. (2008). The secondary permeability of impervious cover. *Environmental & engineering geoscience*, *14*(4), 251-265.

Yariyan, P., Avand, M., Abbaspour, R. A., Torabi Haghighi, A., Costache, R., Ghorbanzadeh, O., Janizadeh, S., & Blaschke, T. (2020). Flood susceptibility mapping using an improved analytic network process with statistical models. *Geomatics, Natural Hazards and Risk*, *11*(1), 2282-2314.

Zhao, G., Pang, B., Xu, Z., Yue, J., & Tu, T. (2018). Mapping flood susceptibility in mountainous areas on a national scale in China. *Science of the Total Environment*, *615*, 1133-1142.

Appendix

Table A1. The regions, amount of flood locations, and variable value classes in the EBF approach

Layer	Classes	Area (%)	Bel	Dis	Unc	Pls
Elevation (Appendix, Figure C1)	402 - 800	39%	0.402	0.129	0.469	0.871
	800 - 1300	37%	0.148	0.251	0.601	0.749
	1300 - 1600	19%	0.171	0.217	0.613	0.783
	1600 - 2000	5%	0.279	0.200	0.520	0.800
	>2000	1%	0.000	0.203	0.797	0.797
Slope (Appendix, Figure C2)	0º – 15º	38%	0.343	0.150	0.507	0.850
	15º – 30º	38%	0.160	0.242	0.598	0.758
	30º – 45º	20%	0.198	0.209	0.593	0.791
	45º – 60º	4%	0.299	0.198	0.503	0.802
	60º – 80º	0%	0.000	0.201	0.799	0.799
Aspect (Appendix, Figure C3)	North	13%	0.052	0.136	0.812	0.864
	Northeast	12%	0.155	0.121	0.724	0.879
	East	10%	0.159	0.121	0.719	0.879
	Southeast	13%	0.244	0.107	0.648	0.893
	South	17%	0.132	0.123	0.744	0.877
	Southwest	15%	0.090	0.131	0.779	0.869
	West	10%	0.088	0.129	0.783	0.871
	Northwest	11%	0.080	0.131	0.790	0.869
Rainfall (Appendix, Figure C4)	700 - 800	23%	0.103	0.226	0.671	0.774
	800 - 900	32%	0.168	0.208	0.623	0.792
	900 - 1000	15%	0.283	0.181	0.536	0.819
	1000 – 1100	13%	0.229	0.192	0.579	0.808
	1100 - 1300	17%	0.216	0.193	0.591	0.807
NDVI (Appendix, Figure C5)	-0.5 to -0.07	22%	0.426	0.147	0.427	0.853
	-0.07 – 0.16	29%	0.226	0.198	0.576	0.802
	0.16 – 0.25	25%	0.142	0.224	0.634	0.776
	0.25 – 0.37	17%	0.094	0.223	0.683	0.777
	0.37 – 0.77	7%	0.112	0.208	0.680	0.792
Geology (Appendix, Figure C6)	Gercus Formation	3%	0.023	0.053	0.923	0.947
	Pilaspi Formation	4%	0.020	0.054	0.927	0.946
	Sehkaniyan and Sarki Formations	1%	0.000	0.053	0.947	0.947
	Chia Gara, Barsarin, Naokelekan and Sargelu Formation	3%	0.028	0.053	0.919	0.947
	Balambo, Garagu and Sarmord Formation	5%	0.033	0.053	0.914	0.947
	Qamchuqa Formation	19%	0.052	0.050	0.898	0.950
	Tanjero Formation	1%	0.052	0.052	0.895	0.948
	Aqra-Bekhme Formation	34%	0.032	0.060	0.908	0.940
	Shiranish Formation	8%	0.092	0.048	0.860	0.952
	Fatha (Lower Fars) Formation	4%	0.000	0.055	0.945	0.945
	Mukdadiyah (Lower Bakhtiari) Formation	3%	0.000	0.054	0.946	0.946
	Injana (Upper Fars) Formation	4%	0.019	0.054	0.927	0.946
	Slope deposits	3%	0.127	0.049	0.824	0.951
	Kolosh Formation	1%	0.000	0.053	0.947	0.947
	Bal Hassan (Upper Bakhtiari) Formation	1%	0.171	0.051	0.778	0.949
	Alluvial fan deposits	4%	0.078	0.051	0.871	0.949
	Flood plain deposits	0%	0.000	0.053	0.947	0.947
	River terraces	0%	0.219	0.052	0.730	0.948
	River	1%	0.053	0.052	0.895	0.948
Soil (Appendix, Figure C7)	Chestnut	8%	0.448	0.192	0.360	0.808
	Lithosols, Rendzinas, Chromic cambisols	62%	0.297	0.135	0.569	0.865
	Lithosols, Rendzinas, Calcic Xerosols, Chromic cambisols	25%	0.070	0.255	0.675	0.745
	Lithosols, Calcaric Regosols, Calcic Xerosols, Chernozems	5%	0.186	0.209	0.605	0.791
	Rough	1%	0.000	0.209	0.791	0.791
Land use (Appendix, Figure C8)	Water Body	1%	0.415	0.196	0.390	0.804
	Forest	25%	0.057	0.240	0.703	0.760
	Built-up	3%	0.158	0.199	0.642	0.801
	Barren Land	59%	0.143	0.183	0.675	0.817

	Cultivated Land	12%	0.228	0.182	0.590	0.818
Distance from Road (Appendix, Figure C9)	0 –25 m	29%	0.333	0.124	0.543	0.876
	25 –50 m	24%	0.195	0.171	0.634	0.829
	50 –75 m	19%	0.153	0.178	0.669	0.822
	75 –100 m	14%	0.079	0.184	0.737	0.816
	100 –125 m	10%	0.146	0.173	0.681	0.827
	>125 m	4%	0.093	0.171	0.736	0.829
Distance from River (Appendix, Figure C10)	0 –50 m	33%	0.495	0.099	0.407	0.901
	50 –100 m	29%	0.184	0.190	0.626	0.810
	100 –150 m	20%	0.196	0.180	0.624	0.820
	150 –200 m	11%	0.126	0.180	0.694	0.820
	200 –250 m	5%	0.000	0.178	0.822	0.822
	>250 m	2%	0.000	0.173	0.827	0.827
Drainage density (Appendix, Figure C11)	0 - 0.56	60%	0.077	0.315	0.608	0.685
	0.56 - 0.86	12%	0.144	0.186	0.670	0.814
	0.86 - 1.43	15%	0.323	0.145	0.533	0.855
	1.43 - 1.72	8%	0.301	0.169	0.530	0.831
	1.72 - 2.0	5%	0.156	0.185	0.659	0.815

Table A2. The final weight of the significant elements represents the flood's potential importance in the AHP technique.

Factors	Factor weight	Class	Class weight	Pixels	Weight (%)
Slope	0.052	0º – 15º	0.020	2847957	38%
		15º – 30º	0.020	2849154	38%
		30º – 45º	0.010	1480220	20%
		45º – 60º	0.002	327470	4%
		60º – 80º	0.000	36494	0%
Aspect	0.027	North	0.003	968570	13%
		Northeast	0.003	870225	12%
		East	0.003	738698	10%
		Southeast	0.003	963574	13%
		South	0.005	1270832	17%
		Southwest	0.004	1122706	15%
		West	0.003	761336	10%
		Northwest	0.003	845354	11%
Elevation	0.035	402 - 800	0.014	2911766	39%
		800 - 1300	0.013	2787192	37%
		1300 - 1600	0.007	1410943	19%
		1600 - 2000	0.002	369680	5%
		>2000	0.000	61714	1%
Rainfall	0.098	700 - 800	0.022	1713774	23%
		800 - 900	0.031	2395279	32%
		900 - 1000	0.015	1156930	15%
		1000 - 1100	0.013	991732	13%
		1100 - 1300	0.017	1283549	17%
Drainage density	0.059	0 - 0.56	0.035	4523909	60%
		0.56 - 0.86	0.007	937667	12%
		0.86 - 1.43	0.009	1133371	15%
		1.43 - 1.72	0.005	575488	8%
		1.72 - 2.0	0.003	370829	5%
Distance from River	0.12	0 –50 m	0.039	2475505	33%
		50 –100 m	0.034	2152474	29%
		100 –150 m	0.023	1471414	20%
		150 –200 m	0.014	859135	11%
		200 –250 m	0.006	403107	5%
		> 250 m	0.003	179629	2%
Land use	0.082	Water Body	0.001	87193	1%
		Forest	0.021	1916937	25%
		Built-up	0.002	228532	3%
		Barren Land	0.048	4435024	59%
		Cultivated Land	0.009	873492	12%
NDVI	0.138	-0.5 to -0.07	0.030	2601235	22%
		-0.07 – 0.16	0.041	3470022	29%
		0.16 – 0.25	0.034	2925801	25%
		0.25 – 0.37	0.023	1964136	17%
		0.37 – 0.77	0.010	822089	7%
Distance from Road	0.038	0 –50 m	0.011	2219874	29%
		50 –100 m	0.009	1819891	24%
		100 –150 m	0.007	1425567	19%
		150 –200 m	0.005	1033994	14%
		200 –250 m	0.004	748374	10%
		> 250 m	0.001	293564	4%
Geology	0.176	Gercus formation	0.006	251405	3%

		Pilaspi formation	0.007	296001	4%
		Sehkaniyan and Sarki formation	0.002	92034	1%
		Chia Gara, Barsarin, Naokelekan and Sargelu formation	0.005	211047	3%
		Balambo, Garagu and Sarmord formation	0.008	353511	5%
		Qamchuqa formation	0.034	1450876	19%
		Tanjero formation	0.003	111483	1%
		Aqra-Bekhme formation	0.059	2548840	34%
		Shiranish formation	0.013	569951	8%
		Fatha (Lower Fars) formation	0.007	282264	4%
		Mukdadiyah (Lower Bakhtiari) formation	0.005	203665	3%
		Injana (Upper Fars) formation	0.007	307547	4%
		Slope deposits	0.005	229963	3%
		Kolosh Formation	0.002	97375	1%
		Bal Hassan (Upper Bakhtiari) formation	0.002	68402	1%
		Alluvial fan deposits	0.007	297859	4%
		Flood plain deposits	0.001	30479	0%
		River terraces	0.001	26734	0%
		River	0.003	110493	1%
Soil	0.175	Chestnut	0.014	585913	8%
		Lithosols, Rendzinas, Chromic cambisols	0.108	4647205	62%
		Lithosols, Rendzinas, Calcic Xerosols, Chromic cambisols	0.044	1876501	25%
		Lithosols, Calcaric Regosols, Calcic Xerosols, Chernozems	0.008	353653	5%
		Rough	0.002	77992	1%
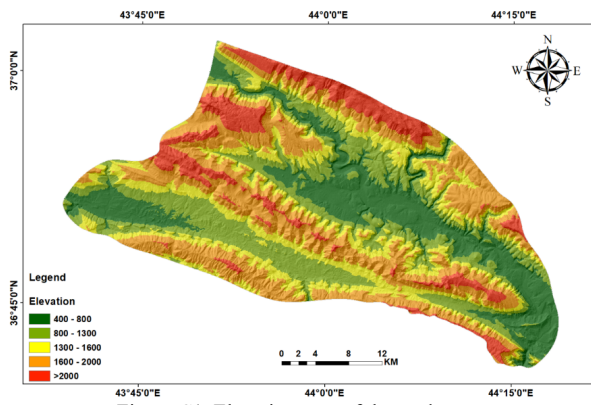
Figure C1. Elevation map of the study area.
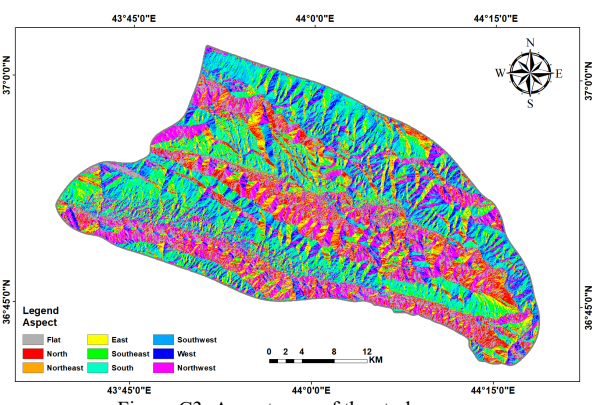
Figure C3. Aspect map of the study area.
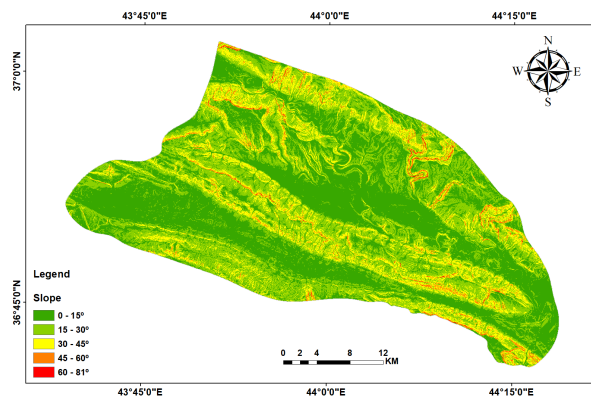
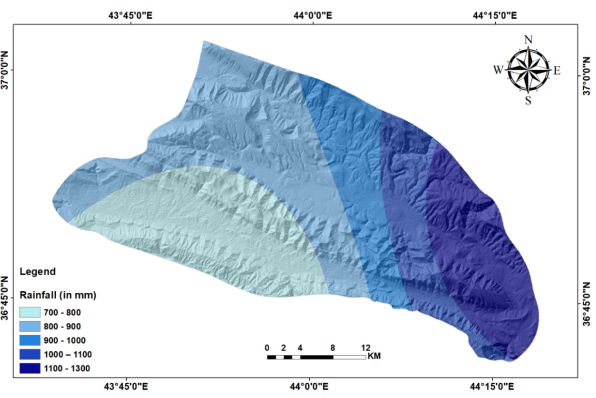Figure C2. Slope map of the study area.
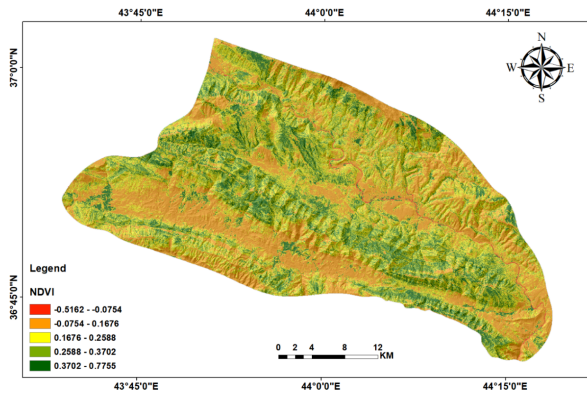

Figure C4. Rainfall map of the study area.

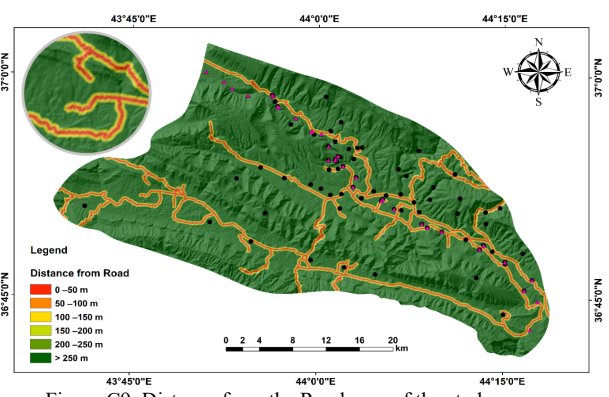Figure C5. NDVI map of the study area

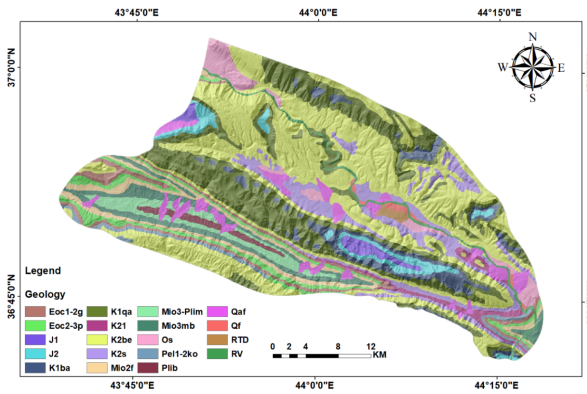Figure C9. Distance from the Road map of the study area.
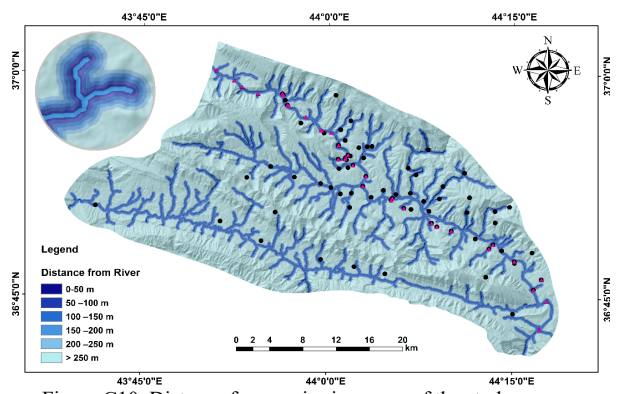

Figure C6. Geology map of the study area.

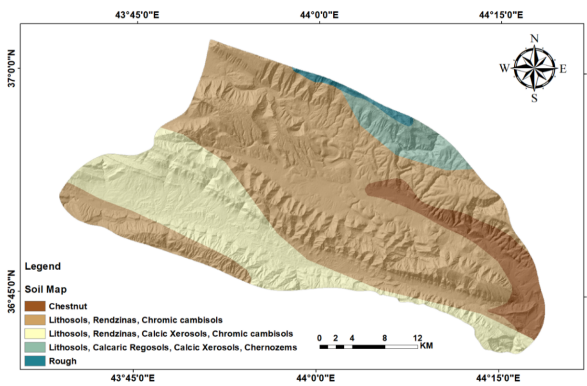Figure C10. Distance from main river map of the study area.

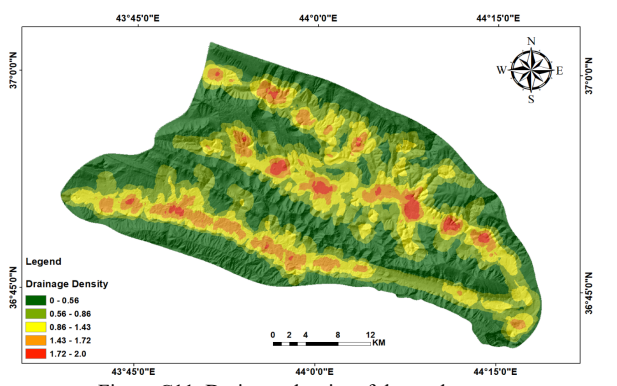Figure C7. soil map of the study area.
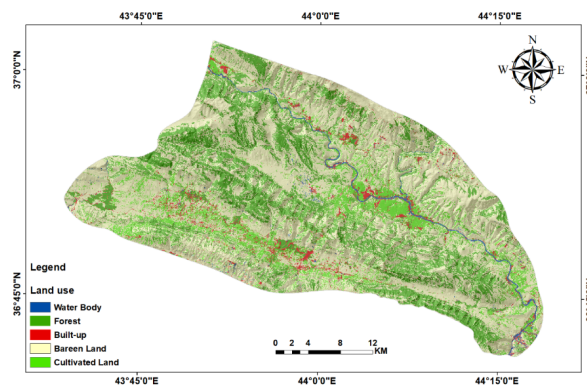

Figure C11. Drainage density of the study area.

Figure C8. Land use and land cover map of the study area.